Cellular Physiology and Biochemistry

Cell Physiol Biochem 2018;49:1717-1733
DOI: 10.1159/000493615
Published online: 20 September, 2018
Accepted: 11 September, 2018

Original Paper

Oxysophocarpine Retards the Growth and Metastasis of Oral Squamous Cell Carcinoma by Targeting the Nrf2/HO-1 Axis

Rui Liu[a,b,c,d] Jia Peng[e] Huili Wang[f] Lei Li[a] Xiujie Wen[c] Yan Tan[a] Lin Zhang[c] Haoyuan Wan[c] Faming Chen[d] Xin Nie[b,g]

[a]State Key Laboratory of Trauma, Burn and Combined Injury, Third Military Medical University, Chongqing, [b]School and Hospital of Stomatology, Wenzhou Medical University, Wenzhou, Zhejiang, [c]Department of Stomatology, Daping Hospital & Research Institute of Surgery, Third Military Medical University, Chongqing, [d]State Key Laboratory of Military Stomatology & National Clinical Research Center for Oral Diseases, Department of Periodontology, School of Stomatology, Fourth Military Medical University, Xi'an, [e]Physical Examination Center, 324th Hospital of PLA, Chongqing, [f]Department of Nursing, Xi'an International University, Xi'an, [g]Department of Maxillofacial Surgery, Daping Hospital & Research Institute of Surgery, Third Military Medical University, Chongqing, China

Key Words
Oral squamous cell carcinoma • Growth • Metastasis • Oxysophocarpine • Nrf2 • HO-1

Abstract
Background/Aims: Nuclear factor erythroid 2-related factor 2 (Nrf2) is an oncogene in various types of cancers, including oral squamous cell carcinoma (OSCC). Oxysophocarpine (OSC) is a natural alkaloid that has multiple pharmacological activities. However, the biological functions and molecular mechanism underlying the effects of OSC on the growth and metastasis of OSCC are unclear. ***Methods:*** Nrf2 levels were determined in OSCC tissues and non-cancerous specimens by quantitative real-time PCR, western blotting, and immunohistochemistry (IHC) assays. The effects of OSC on OSCC cell growth and metastasis were explored (1) using 5-ethynyl-20-deoxyuridine staining and Cell Counting Kit-8, colony formation, flow cytometry, wound-healing, Transwell, and tube formation assays *in vitro*; and (2) by establishing a xenograft nude mouse model *in vivo*. The molecular mechanisms underlying the effects of OSC on the growth and metastasis of OSCC were investigated *in vitro* by western blotting, caspase-3 activity, and enzyme-linked immunosorbent assays, and *in vivo* by western blotting and IHC assays. ***Results:*** The expression levels of Nrf2 in OSCC tissues and in cell lines were much higher than in non-cancerous tissues and normal oral keratinocytes. The upregulation of Nrf2 was positively correlated with a high incidence of lymph node metastasis and advanced histological grade and TNM stage, but inversely associated with differentiation and survival of

R. Liu and J. Peng contributed equally to this work.

Xin Nie, MD
Wenzhou Medical University, School and Hospital of Stomatology
373 College West Road, Wenzhou, Zhejiang 325035 (China)
Tel. +86-577-56953758, Fax +86-577-56953758, E-Mail xinnie163@163.com

OSCC patients. OSC reduced the expression of Nrf2 and heme oxygenase 1 (HO-1) in OSCC cells. OSC also inhibited proliferation, migration, invasion, and pro-angiogenesis of OSCC cells. Moreover, OSC induced cell cycle arrest, enhanced apoptosis of OSCC cells *in vitro*, and decreased OSCC tumor growth *in vivo*. Mechanically, OSC reduced the aggressive behavior of OSCC cells by inactivation of the Nrf2/HO-1 signaling pathway. ***Conclusion:*** Our findings provide evidence that OSC inhibits the growth and metastasis of OSCC by targeting the Nrf2/HO-1 axis, suggesting that OSC may be a potential therapeutic agent for OSCC.

Introduction

Oral squamous cell carcinoma (OSCC), the major type (> 90%) of oral cancer worldwide, is one of the most aggressive cancers [1, 2]. The well-established etiological factors of OSCC include tobacco usage, alcohol consumption, betel quid chewing, and human papillomavirus infection [3, 4]. Despite considerable improvements in the combination of surgery, radiotherapy, and chemotherapy, the 5-year survival rate of OSCC patients remains less than 50% [5]. Excessive proliferation, local invasion, distant metastasis, and recurrence are considered the most important adverse prognostic factors for OSCC [6, 7]. Thus, the molecular mechanisms underlying OSCC progression and effective therapeutic agents against OSCC need to be explored.

Nuclear factor erythroid 2-related factor 2 (Nrf2) is a redox-sensitive transcription factor that controls the expression of various antioxidant and cytoprotective genes regulating the cellular response to oxidative and electrophilic stresses [8]. Under basal conditions, Nrf2 is sequestered by the Kelch-like ECH-associated protein 1 (Keap1), which is a Cul3-based E3 ubiquitin ligase adapter that leads to Nrf2 ubiquitination and proteasome-dependent degradation [9]. Under conditions of oxidative stress, Keap1 is modified and allows Nrf2 to be released and translocate into the nucleus where it recognizes an enhancer sequence known as the antioxidant-response element, resulting in the transcription of antioxidants, phase II detoxification enzymes, and drug transporters [10-12]. Nrf2 is a primary cellular defense protein against the cytotoxic effects of oxidative stress; thus, Nrf2 has been traditionally considered as a tumor suppressor [13]. However, mounting evidence revealed the potential oncogenic roles of Nrf2 and its transcriptional target genes, such as heme oxygenase 1 (HO-1) [14, 15], one of the main effectors of Nrf2-dependent cell responses [15]. Nrf2 is highly expressed in many types of tumors, including OSCC [16-22]. Moreover, the enhancement of Nrf2 expression can be considered a poor prognostic factor [16, 17]. Nrf2/HO-1 signaling activation promotes metastasis, angiogenesis, and chemotherapy and radiotherapy resistance of cancer cells [14, 15]. Fan et al [23]. showed that Nrf2 overexpression increases proliferation, migration, and invasion of OSCC cells by regulating Notch signaling. However, the functional roles of the Nrf2/HO-1 axis in the regulation of aggressive phenotypes of OSCC are largely unknown.

Oxysophocarpine (OSC) is a quinolizidine alkaloid isolated from *Sophora flavescens* Ait. (Kushen), *S. alopecuroides* L. (Kudouzi or Kugancao), and other leguminous plants of the genus Robinia [24]. OSC is a widely used traditional Chinese medicine and has anti-nociceptive [25], neuroprotective [26, 27], analgesic [28], and anti-viral [29, 30] activities through anti-apoptotic, anti-inflammatory, and immunosuppressive effects. OSC has been demonstrated to exert anti-cancer activity, but few studies have focused on the effects of OSC on cancer [31]. Previously, OSC was reported to suppress the proliferation and promote the apoptosis of PC-3 prostate cancer cells [32]. However, whether OSC produces anti-OSCC effects remains unclear.

In this study, Nrf2 was highly expressed in OSCC tissues and cell lines. Increased expression of Nrf2 was positively associated with lymphatic and distant metastases, high histological grades, and advanced stages, but negatively associated with tumor differentiation and the prognosis of OSCC patients. OSC suppressed the activation of Nrf2/HO-1 signaling in OSCC cells. Functional studies demonstrated that OSC reduced the proliferation, apoptosis escape,

migration, invasion, and pro-angiogenesis of OSCC cells *in vitro* in an HO-1-dependent manner. The results of *in vivo* studies were highly consistent with the findings *in vitro*. Collectively, our results revealed that OSC exerts remarkable effects on anti-proliferation, pro-apoptosis, anti-motility, and anti-angiogenesis in OSCC cells, potentially providing evidence for developing this natural product as a therapeutic agent for OSCC.

Table 1. Correlation between Nrf2 expression and clinicopathological characteristics in OSCC patients. *P < 0.05

Variables	Clinicopathological parameters	Case No. (n = 96)	Nrf2 expression		P value
			High (n = 56)	Low (n = 40)	
Sex	Male	56	31	25	0.786
	Female	40	25	15	
Age (years)	< 60	59	36	23	0.628
	≥ 60	37	20	17	
Smoking	Yes	54	31	23	0.521
	No	42	25	17	
Alcohol consuption	Yes	61	37	24	0.342
	No	35	19	16	
Differentiation	High/moderate	63	36	27	0.038*
	Low	33	20	13	
Clinical stage	I/II	61	30	31	0.005*
	III/IV	35	26	9	
pT stage	T1/T2	64	32	32	0.016*
	T3/T4	32	24	8	
pN stage	N0/N1	54	26	28	0.003*
	N2/N3	42	30	12	
pM stage	M0	85	46	39	< 0.001*
	M1	11	10	1	

Materials and Methods

Patients and samples

Cancer and corresponding non-cancerous tissue samples were obtained from 96 OSCC patients who underwent surgical resection at the School and Hospital of Stomatology, Wenzhou Medical University between July 2008 and April 2012; the follow-up period for survival analyses ended in April 2017. None of the patients received preoperative chemotherapy or radiotherapy, and written informed consent was obtained from all patients. This study was approved by the ethics committee of Wenzhou Medical University, and all the experimental procedures were performed in accordance with the National Institutes of Health guidelines. The tumor tissues were analyzed by pathological examination and classified using the World Health Organization classification system; clinical stage was determined by the tumor–node–metastasis (TNM) classification of the American Joint Committee on Cancer. Clinicopathological characteristics of the patients are summarized in Table 1. A total of 96 pairs of paraffin-embedded cancer and non-cancerous tissue specimens were collected for immunohistochemistry (IHC) staining and 30 pairs of freshly isolated OSCC and the corresponding non-cancerous tissues were stored in liquid nitrogen for quantitative real-time PCR (qPCR) assay and western blot analysis.

Cell culture, transfection, and treatment

Five human OSCC cell lines (Tca8113, Cal27, SCC-9, SCC-15, and SCC-25) were purchased from American Type Culture Collection (ATCC; Manassas, VA) and cultured in Dulbecco's modified Eagle's medium (DMEM; Gibco BRL, Carlsbad, CA). Human normal oral keratinocytes (hNOKs; ScienCell Research Laboratories, Carlsbad, CA) were maintained in oral keratinocyte medium (ScienCell Research Laboratories). Human umbilical vein endothelial cells (HUVECs; ATCC) were cultivated in M200 medium (Cascade Biologics, Portland, OR). All cell lines were supplemented with 10% fetal bovine serum (FBS; Gibco BRL), 100 U/ml penicillin, and 100 μg/ml streptomycin (Sigma-Aldrich, St. Louis, MO) in a humidified atmosphere with 5% CO_2 at 37°C. The small interfering RNA-targeting Nrf2 (siNrf2), HO-1 (siHO-1), and the negative control siRNA (siNC) were synthesized by GenePharma (Shanghai, China) and transfected into SCC-9 and SCC-15 cells using Lipofectamine 2000 (Invitrogen, Carlsbad, CA) in accordance with the manufacturer's

instructions. SCC-9 and SCC-15 cells were treated with vehicle control, OSC (3, 5, or 7 μM; Ningxia Institute of Materia Medica, Yinchuan, China), or zinc protoporphyrin (ZnPP; 10 μM; Sigma-Aldrich) for 24 h, and the treated cells were further investigated.

qPCR assay

Total RNA was isolated from fresh tissues and cultured cells using TRIzol reagent (Invitrogen) according to the manufacturer's instructions. Reverse transcription was performed with 1 μg total RNA using the PrimeScript RT Reagent Kit (Takara, Dalian, China). The qPCR assay was performed using an ABI 7500 real-time PCR system (Applied Biosystems, Foster City, CA) with a SYBR Green Real-time PCR Kit (Takara). Glyceraldehyde 3-phosphate dehydrogenase (GAPDH) was used as an internal control. The relative expression of Nrf2 was calculated using the $2^{-\Delta\Delta Ct}$ method. The following primers were used: for Nrf2, forward 5′-AGCAGGCTGAGACTACCACT-3′ and reverse 5′-TCCAGTGAGGGGATCGATGA-3′; for GAPDH, forward 5′-CATCTCTGCCCCCTCTGCTGA-3′ and reverse 5′-GGATGACCTTGCCCACAGCCT-3′.

Western blot analysis

Protein was extracted from tissue specimens and cultured cells using RIPA lysis buffer (Beyotime, Shanghai, China) and the concentration was determined using a BCA Protein Assay Kit (Beyotime). Equal amounts of protein samples were separated by sodium dodecyl sulfate-polyacrylamide gel electrophoresis and then transferred onto polyvinylidene-fluoride membranes (Millipore, Bedford, MA). After blocking with 5% non-fat milk in Tris-buffered saline and Tween 20 for 1 h at room temperature, the membranes were incubated with primary antibodies against Nrf2, HO-1, proliferating cell nuclear antigen (PCNA), cyclin D1, Bcl-2, Bax (Abcam, Cambridge, UK), E-cadherin, vimentin, matrix metalloproteinase-9 (MMP-9), hypoxia-inducible factor 1α (HIF-1α), vascular endothelial growth factor (VEGF), and GAPDH (Cell Signaling Technology Beverly, MA) at 4°C overnight, followed by incubation with horseradish peroxidase (HRP)-conjugated secondary antibodies (Abcam) at 37°C for 1 h. GAPDH was used as the loading control. Protein bands were analyzed using an enhanced chemiluminescence kit (Pierce Biotechnology, Rockford, IL) with an imaging system (Bio-Rad Laboratories, Hercules, CA).

IHC staining

Paraffin-embedded tissues were sectioned (4 μm thick), deparaffinized with xylene, and dehydrated in a series of graded ethanol solutions. Endogenous peroxidase activity was quenched with 3% hydrogen peroxide at room temperature for 15 min, and the sections were then boiled in citrate buffer for 10 min at 121°C in a microwave oven to retrieve antigenicity. The sections were incubated with primary antibodies against Nrf2, HO-1, PCNA, cyclin D1, Bcl-2, Bax, E-cadherin, vimentin, MMP-9, HIF-1α, and VEGF at 4°C overnight, followed by incubation with a biotin-labeled secondary antibody (Vector Laboratories, Burlingame, CA) at 37°C for 1 h. Sections were stained with diaminobenzidine, counterstained with hematoxylin, and observed under a light microscope (Olympus, Tokyo, Japan). Immunostaining was classified into two groups according to intensity and extent. Intensity scores were expressed as follows: 0, negative staining; 1, weak staining; 2, moderate staining; and 3, strong staining. Extent scores (percentage of tumor cells stained positive) were represented as follows: 0, < 20% of cells; 1, 20% to 50% of cells; and 3, > 50% of the cells. The final staining score (intensity × extent) varied from 0 to 9 for each spot. According to the final scores, the tissues were divided into two groups: Nrf2 low expression group (score ≤ 3) and Nrf2 high expression group (score > 3).

Cell viability assay

Cell viability was measured using the Cell Counting Kit-8 (CCK-8) assay (Dojindo Laboratories, Tokyo, Japan) according to the manufacturer's protocol. After different treatments, SCC-9 and SCC-15 cells were seeded in 96-well plates at a density of 1×10^3/well and cultured for 1, 2, 3, and 4 days. CCK-8 reagents (10 μl) were added to each well at the indicated time points and incubated for 1 h. Cell viability was determined by measuring the absorbance at 450 nm using a microplate reader (Bio-Rad Laboratories).

5-Ethynyl-20-deoxyuridine incorporation assay

Cell proliferation was assessed using a *5-ethynyl-20-deoxyuridine* (EdU) incorporation assay following the manufacturer's instructions. Briefly, SCC-9 and SCC-15 cells were seeded in six-well plates and subjected to different treatments for 24 h. EdU (50 μM; RiboBio, Guangzhou, China) was added into each well, and cells were cultured for 2 h, followed by fixing with 4% paraformaldehyde for 20 min at room temperature. The plates were observed and photographed under an inverted fluorescent microscope (Olympus).

Colony formation assay

For colony formation assay, SCC-9 and SCC-15 cells subjected to various treatments were plated in six-well plates at a density of 1×10^3/well and incubated in DMEM containing 10% FBS at 37°C for 14 days in a humidified chamber with 5% CO_2. Fresh culture medium was replaced every 2 days. The cells were then fixed with methanol and stained with 0.1% crystal violet (Sigma-Aldrich). Colony formation was determined by counting the number of visible colonies.

Cell cycle analysis

The cell cycle was analyzed by flow cytometry. In brief, SCC-9 and SCC-15 cells subjected to various treatments were harvested and fixed with 70% cold ethanol for 2 h. RNasw was added (1 mg/ml; Takara) and cells were incubated at 37°C for 30 min. Intracellular DNA was labeled with 50 μg/ml propidium iodide (PI; Sigma-Aldrich) at 4°C for 30 min. The samples were assayed using a FACScan flow cytometer (BD Biosciences, San Jose, CA). The results were analyzed using CELL Quest 3.0 software (BD Biosciences).

Apoptosis assay by flow cytometry

Cell apoptosis was analyzed by flow cytometry using an Annexin V/Fluorescein isothiocyanate (FITC) and PI Apoptosis Detection Kit (BD Biosciences) according to the manufacturer's protocol. In brief, SCC-9 and SCC-15 cells subjected to different treatments were harvested, centrifuged, and resuspended in 1× binding buffer at a final concentration of 1×10^6 cells/ml. Annexin V/FITC (10 μl) was added in the mixture, incubated at 37°C for 15 min, and counterstained with PI (5 μl) in the dark for 30 min. Annexin V/FITC and PI fluorescence were determined using the FACSCalibur flow cytometer. Results were analyzed using CELL Quest 3.0 software.

Caspase-3 activity assay

Caspase-3 activity was measured using the Caspase-3/CPP32 Colorimetric Assay Kit (BioVision, Palo Alto, CA) in accordance with the manufacturer's instruction. After various treatments, SCC-9 and SCC-15 cells (1×10^6) were lyzed, and the supernatant was collected. Protein (150 μg) was added to 2× reaction buffer containing 5 μl N-Acetyl-Asp-Glu-Val-Asp-pNA substrate (200 μM final concentration) and incubated at 37°C for 2 h. N-Acetyl-Asp-Glu-Val-Asp-pNA cleavage was determined by measuring enzyme-catalyzed release of pNA at 405 nm using a microplate reader (Bio-Rad Laboratories).

Wound-healing assay

SCC-9 and SCC-15 cells subjected to various treatments were seeded in six-well plates and incubated for 24 h in a humidified chamber with 5% CO_2 at 37°C. Wounds were made using a 200-μl pipette tip on a confluent cell monolayer. The cells were continuously incubated for 48 h, and wound closure was observed. Photographs were captured at 0 and 48 h with a phase-contrast microscope (Olympus).

Transwell assays

Cell migration and invasion were assessed by Transwell assays. For the migration assay, SCC-9 and SCC-15 cells subjected to various treatments were seeded into the upper chamber of the Transwell apparatus (8-μm pore size; Corning Costar, Dallas, TX) with serum-free DMEM. The lower chamber was filled with DMEM containing 15% FBS as a chemoattractant. The procedure for the invasion assay was similar to that of the migration assay, except that the Transwell membranes were pre-coated with 200 μg/ml Matrigel (BD Biosciences). After incubation for 24 h, cells that had migrated or invaded through the membrane were fixed with methanol, stained with crystal violet, and counted using a microscope (Olympus).

Tube formation assay

In vitro angiogenesis was determined using the tube formation assay. HUVECs (1×10^5) were seeded into 24-well plates pre-coated with Matrigel and cultured in M200 medium containing 50 µl conditioned medium (CM) freshly collected from SCC-9 and SCC-15 cells subjected to various treatments. After incubation for 36 h, tube formation was monitored and photographed under a phase contrast microscope (Olympus). The tube number, tube branch points, and relative tubule length were determined.

Enzyme-linked immunosorbent assay

VEGF release from SCC-9 and SCC-15 cells subjected to various treatments was measured by enzyme-linked immunosorbent assay (ELISA) using a commercial kit (R&D Systems, Minneapolis, MN) according to the manufacturer's instructions. In brief, cell supernatants or standards (200 µl) were added to the microplate pre-coated with monoclonal antibody against VEGF and incubated for 2 h at room temperature, followed by incubation with HRP-conjugated secondary antibody for 2 h at room temperature. Substrate solution was then added and cells were incubated for 30 min until stop solution was added to stop the reaction. The absorbance was measured at 450 nm on a microplate reader (Bio-Rad Laboratories). Results were expressed as pg/ml.

In vivo xenograft tumor model

Six-week-old male BALB/c nude mice (weighing 22–24 g) were purchased from the Institute of Zoology, Chinese Academy of Sciences, Beijing, China and maintained on a standard diet and water under pathogen-free conditions with a regular 12-h day/night cycle. All the experimental procedures were approved by the Institutional Guidelines of Animal Care and Use Committee of Wenzhou Medical University.

For the xenograft tumor formation assay, SCC-9 cells (3×10^6) mixed with Matrigel were subcutaneously injected into the flanks of mice. When tumor size reached approximately 60 mm^3, the mice were randomly assigned to control and OSC groups (n = 6 per group). OSC (80 mg/kg) or vehicle control was administered by intraperitoneal injection every 2 days for 3 weeks. Tumor size was monitored once a week, and tumor volume was determined using the formula: tumor volume = (length × $width^2$)/2. Six weeks after SCC-9 cell implantation, the animals were killed, and the tumors were immediately collected and weighed. The tumor tissues were fixed with 4% paraformaldehyde and embedded in paraffin for IHC staining or stored at –80°C for western blot analysis.

Statistical analysis

All statistical analyses were performed using the GraphPad Prism 5.0 statistical software package (GraphPad Software, Inc. La Jolla, CA). All data are expressed as the mean ± standard deviation (SD). Differences were analyzed using Student's *t* test between two groups or one-way analysis of variance for multiple groups. Survival curves were plotted using the Kaplan–Meier method and analyzed using the log rank test. Chi-squared test was used to analyze the relationship between Nrf2 levels and clinicopathological characteristics of patients. $P < 0.05$ was considered statistically significant.

Results

Upregulation of Nrf2 is positively associated with tumor progression and poor prognosis of OSCC patients

To explore the relationship between Nrf2 expression and OSCC, we measured the mRNA levels of Nrf2 in 30 pairs of OSCC and the corresponding non-cancerous tissue samples by qPCR. As shown in Fig. 1A, the mRNA level of Nrf2 was significantly increased in OSCC tissues compared with non-cancerous samples. Moreover, patients with lymphatic metastasis or tumors at advanced histological grades (III/IV) had higher levels of Nrf2 mRNA compared with cases with non-metastatic or low-stage (I/II) tumors (Fig. 1B–C; Table 1). Upregulation of Nrf2 was also closely correlated with differentiation and TNM stage but not significantly associated with sex, age, smoking, and alcohol consumption (Table 1). The results of western blotting showed that the protein level of Nrf2 was much higher in OSCC tissues than in non-cancerous samples (Fig. 1D). IHC results also indicated high expression of Nrf2

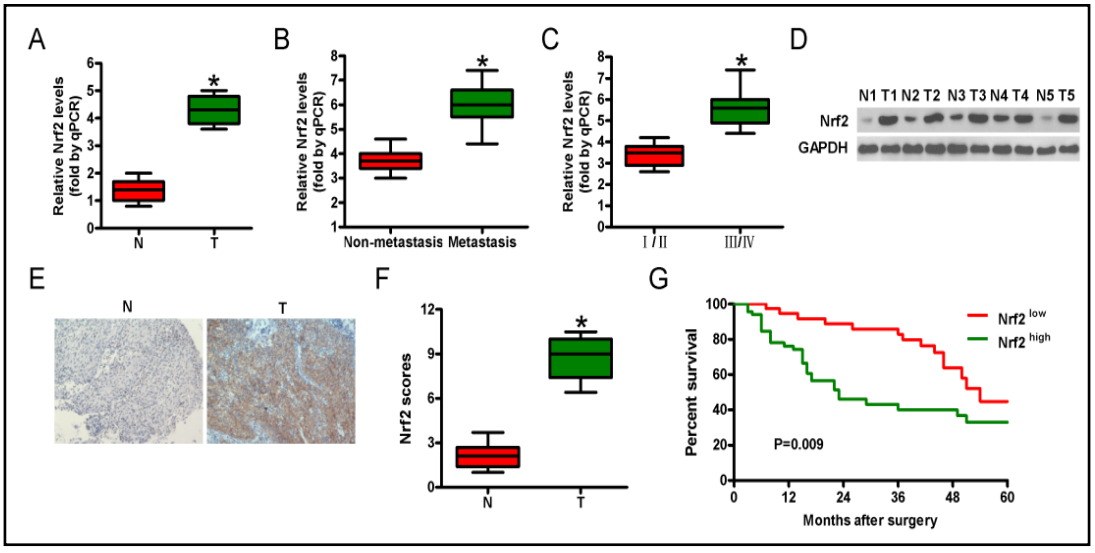

Fig. 1. Expression of Nrf2 in OSCC tissues and cell lines and its correlation with lymph node metastasis, histological grades, and survival of OSCC patients. (A) Nrf2 expression was measured by qPCR assay in 30 pairs of OSCC and the corresponding non-cancerous tissues. GAPDH was used as the normal control. Comparisons of Nrf2 levels in OSCC patients (B) with (n = 42) or without (n = 54) lymphatic metastasis and (C) with tumors of different grades (I/II, n = 61; III/IV, n = 35). GAPDH was used as the normal control. (D) Representative western blotting results of Nrf2 expression in five pairs of OSCC and the corresponding non-cancerous tissues. GAPDH was used as the endogenous control. Representative images of (E) Nrf2 IHC staining and (F) Nrf2 expression scores in 96 pairs of OSCC and non-cancerous tissue samples. (G) Five-year survival rate of OSCC patients with high (n = 56) and low Nrf2 expression (n = 40). All data are presented as the mean ± SD of three replicates. *P<0.05 compared with N group in (A and D), non-metastatic group in (E), and I/II grades in (F). N: non-cancerous samples; T: OSCC tissues.

in OSCC tissues (Fig. 1E–F). Furthermore, patients with high Nrf2 expression had poorer survival than those with low Nrf2 expression levels (Fig. 1G). These results suggest that Nrf2 elevation plays a key role in the development and progression of OSCC and may be a useful prognostic marker for OSCC.

OSC inhibits the Nrf2/HO-1 signaling pathway in OSCC cells

The baseline mRNA and protein expression levels of Nrf2 in the hNOKs and five OSCC cell lines (Tca8113, Cal27, SCC-9, SCC-15, and SCC-25) were measured by qPCR and western blotting assays. Nrf2 was highly expressed both at the mRNA and protein levels in the five OSCC cell lines compared with hNOKs (Fig. 2A–B). SCC-9 and SCC-15 cells were selected for subsequent studies because they had the highest Nrf2 levels among the five OSCC cell lines. To evaluate the effect of OSC on Nrf2 and HO-1 expression, we treated SCC-9 and SCC-15 cells with the vehicle control or 3, 5, and 7 μM OSC for 24 h. Nrf2 and HO-1 protein expression levels were decreased in a dose-dependent manner in the SCC-9 and SCC-15 cells, and 5 and 7 μM OSC treatment had similar effects on Nrf2 and HO-1 expression. Thus, 5 μM OSC was selected for subsequent experiments (Fig. 2C). To verify HO-1 as a target of Nrf2 in OSCC cells, we transfected SCC-9 and SCC-15 cells with siNC or siNrf2 mimics. As shown in Fig. 2D, siNrf2 transfection led to significant reduction in Nrf2 and HO-1 expression compared with siNC-transfected or control cells. These data demonstrate that OSC suppresses Nrf2 and HO-1 expression in OSCC cells.

OSC induces proliferation inhibition and apoptosis of OSCC cells

To determine the functional role of OSC in cell proliferation, we performed the CCK-8 assay, EdU staining, and colony formation assays. OSC treatment significantly inhibited the viability of SCC-9 and SCC-15 cells compared with control cells (Fig. 3A). EdU staining demonstrated a reduction in proliferative SCC-9 and SCC-15 cells in the OSC-treated group (Fig. 3B–C). The colony formation assays showed substantial reduction in the colonies of OSC-treated SCC-9 and SCC-15 cells (Fig. 3D–E). OSC administration reduced cell cycle transition from G1 to S phase in SCC-9 and SCC-15 cells compared with the corresponding control cells (Fig. 3F–G). Next, we explored the effect of OSC on apoptosis of OSCC cells. As shown in Fig. 3H–I, flow cytometry assay indicated that OSC treatment resulted in more apoptotic cells compared with the control SCC-9 and SCC-15 cells. OSC treatment significantly increased caspase-3 activity in SCC-9 and SCC-15 cells (Fig. 3J). These results indicate that OSC inhibits OSCC cell proliferation and induces apoptosis.

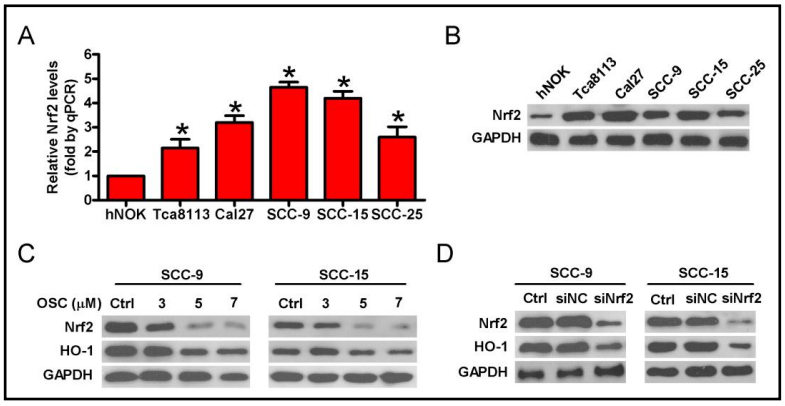

Fig. 2. OSC inhibited Nrf2 and HO-1 expression in OSCC cells. (A) mRNA and (B) protein expression levels of Nrf2 in five OSCC cell lines and hNOKs were measured by qPCR and western blotting. (C) SCC-9 and SCC-15 cells were treated with vehicle control or 3, 5, and 7 μM OSC for 24 h. Nrf2 and HO-1 protein expression levels were determined by western blotting. (D) SCC-9 and SCC-15 cells were non-transfected (control) or transfected with 100 nM siNrf2 or siNC mimics for 48 h. Western blotting was performed to analyze the expression of Nrf2 and HO-1. GAPDH was used as the endogenous control. *P<0.05 compared with hNOK cells. Ctrl: control.

OSC suppresses migration and invasion of OSCC cells

To investigate the effects of OSC on OSCC cell mobility, we performed wound-healing and Transwell assays. As shown in Fig. 4A–B, the wound-healing assay showed that OSC treatment markedly reduced SCC-9 and SCC-15 cell migration compared with the control cells. The reduction in migratory cells caused by OSC was also evidenced by the Transwell assay (Fig. 4C–D). Moreover, the invasion of SCC-9 and SCC-15 cells was suppressed by OSC treatment (Fig. 4E–F). These findings suggest that OSC decreases migration and invasion of OSCC cells.

OSC reduces the pro-angiogenic effects of OSCC cells

To examine whether OSC has anti-angiogenic effects on OSCC cells, we treated SCC-9 and SCC-15 cells with OSC or vehicle control for 24 h, and the CM was collected to incubate HUVECs for tube formation assays. As expected, fewer tube formations were observed for HUVECs treated with the CM from OSC-treated SCC-9 and SCC-15 cells compared with control cells (Fig. 5A). The tube number (Fig. 5B), tube branch points (Fig. 5C), and tube length (Fig. 5D) were considerably reduced in the HUVECs cultured with OSC-treated CM. The secretion of pro-angiogenic growth factor VEGF was also reduced by OSC treatment in SCC-9 and SCC-15 cells (Fig. 5E). These data suggest that OSC reduces pro-angiogenesis of OSCC cells.

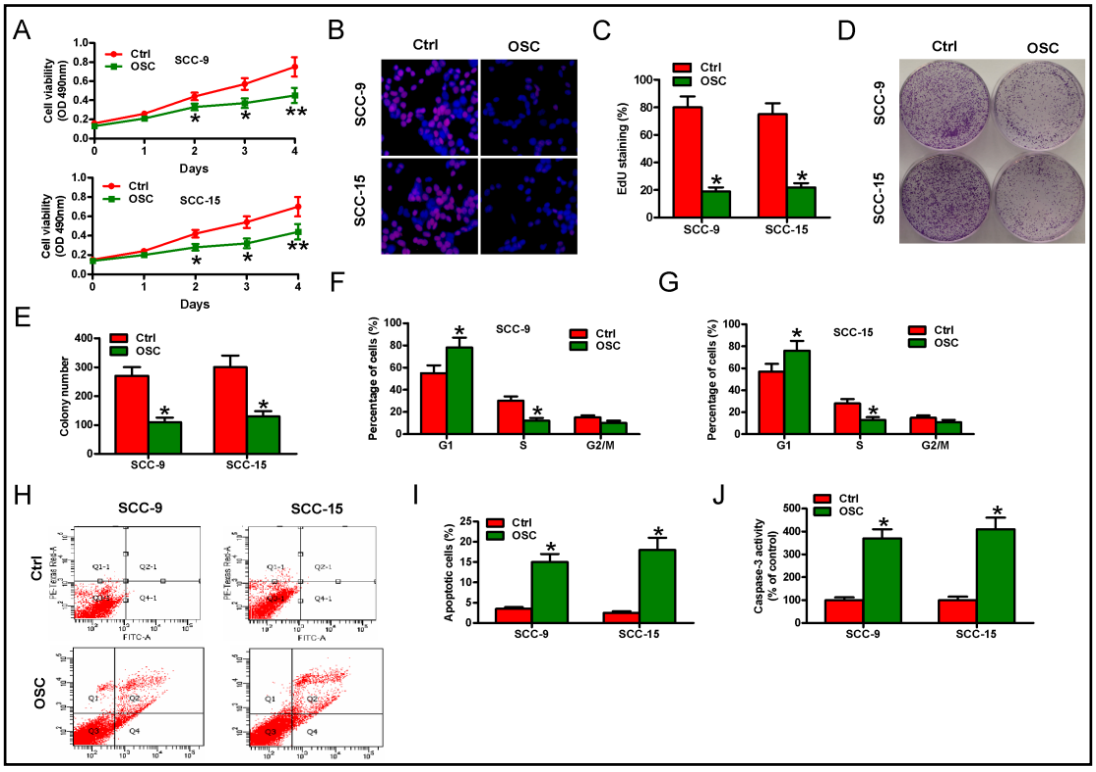

Fig. 3. OSC reduced the proliferation of and induced apoptosis in OSCC cells. SCC-9 and SCC-15 cells were treated with 5 μM OSC or vehicle control for 24 h. (A) CCK-8 assay was performed to analyze cell viability. (B) EdU staining was performed to assess cell proliferation. (C) The percentage of EdU-positive cells was calculated. (D) Cell proliferation was measured by colony formation assay. (E) Colony formation number was calculated. (F and G) Cell cycle was analyzed by flow cytometry and the cell cycle distribution was calculated as a percentage. (H) Flow cytometry was performed to determine cell apoptosis. (I) Percentage of apoptotic cells. (J) Caspase-3 activity was measured to evaluate cell apoptosis. Data are presented as the mean ± SD of three independent experiments. *P<0.05, **P<0.01 versus Ctrl group. Ctrl: control.

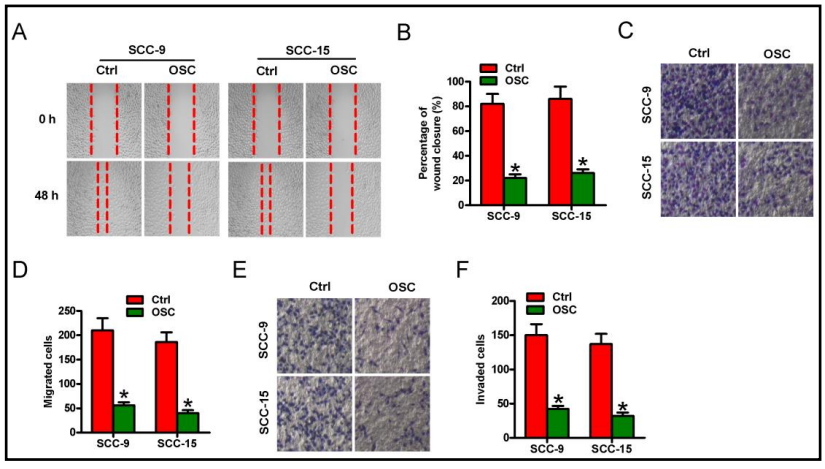

Fig. 4. OSC suppressed migration and invasion of OSCC cells. SCC-9 and SCC-15 cells were treated with 5 μM OSC or vehicle control for 24 h. (A) Wound-healing assay was performed to evaluate cell migration. (B) Wound closure was calculated as a percentage. (C) Migration and (E) invasion were determined by Transwell assays. The numbers of (D) migrated and (F) invaded cells were counted. Data are presented as the mean ± SD of three independent experiments. *P<0.05 versus Ctrl group. Ctrl: control.

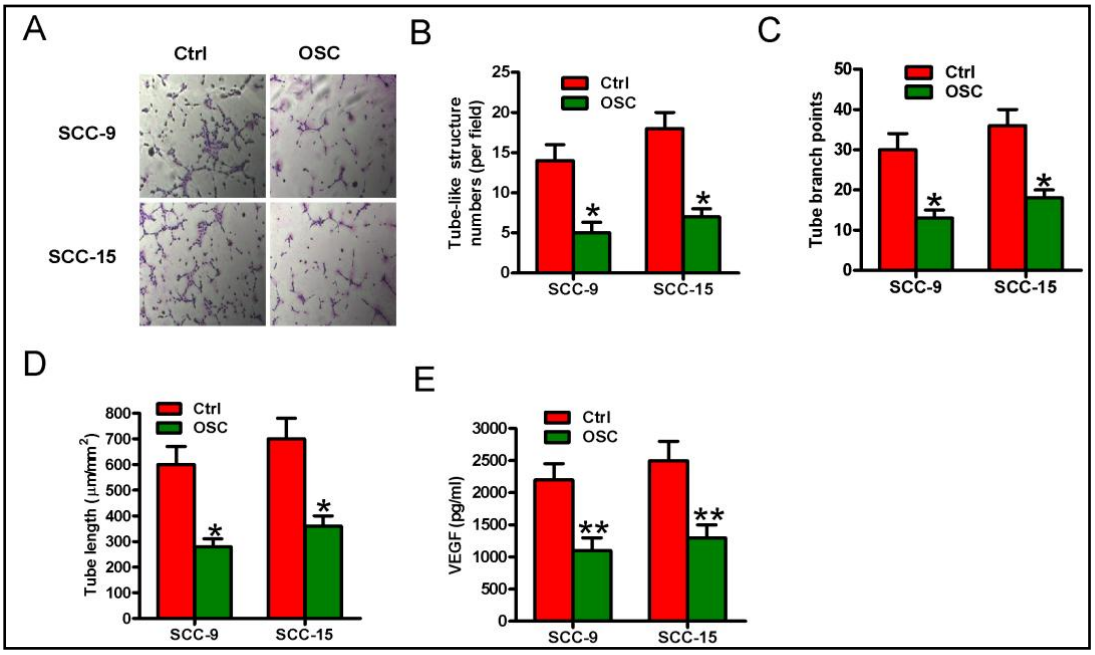

Fig. 5. OSC reduced vasculogenic mimicry of OSCC cells. (A–D) SCC-9 and SCC-15 cells were treated with 5 μM OSC or vehicle control for 24 h and the CM was harvested to incubate HUVECs for 36 h. (A) Representative images of tube formation. (B) Tube number, (C) tube branch points, and (D) tube length were determined. (E) SCC-9 and SCC-15 cells were treated with 5 μM OSC or vehicle control for 24 h. The supernatants were collected for VEGF measurement using ELISA. Data are presented as the mean ± SD of three independent experiments. *P<0.05, **P<0.01 versus Ctrl group. Ctrl: control.

OSC exerts anti-OSCC effects by inactivating HO-1 signaling

Next, we investigated whether OSC inhibited the proliferation of and facilitated apoptosis in OSCC cells via inactivation of HO-1 signaling. The colony formation assay showed substantial reduction in the colonies of SCC-9 and SCC-15 cells treated with OSC, siHO-1. or the HO-1 inhibitor ZnPP (Fig. 6A). OSC, siHO-1, or ZnPP treatment significantly increased caspase-3 activity in SCC-9 and SCC-15 cells (Fig. 6B). Molecular analyses demonstrated that OSC reduced the expression levels of pro-survival proteins including HO-1, PCNA, cyclin D1, and Bcl-2, and enhanced the levels of the pro-apoptotic protein Bax in SCC-9 and SCC-15 cells (Fig. 6C). Then, we examined the effects of siHO-1 and ZnPP on the expression levels of these proteins. We found that siHO-1 transfection or ZnPP treatment downregulated the levels of PCNA, cyclin D1, and Bcl-2, and upregulated the expression of Bax in SCC-9 and SCC-15 cells, similar to the effects of OSC (Fig. 6C). Furthermore, we addressed whether OSC hindered the HO-1 signaling-dependent migration and invasion of OSCC cells. As shown in Fig. 6D–E, Transwell assays demonstrated that OSC, siHO-1, or ZnPP treatment markedly decreased SCC-9 and SCC-15 cell migration and invasion compared with control cells. OSC administration resulted in upregulation of E-cadherin and downregulation of HO-1, vimentin, and MMP-9 in SCC-9 and SCC-15 cells (Fig. 6F). In addition, ZnPP treatment or transfection with siHO-1 led to higher expression of E-cadherin and lower levels of vimentin and MMP-9 in SCC-9 and SCC-15 cells compared with the siNC-transfected or control cells, consistent with the effects of OSC (Fig. 6F). Then, we investigated whether OSC-suppressed vasculogenic mimicry was dependent on HO-1 signaling. Tube formation assays showed fewer tube formations for HUVECs treated with the CM from SCC-9 and SCC-15 cells treated with OSC, si-HO-1, or ZNPP compared with HUVECs treated with CM from control cells (Fig. 6G). VEGF release was also reduced by OSC, si-HO-1, or ZnPP treatment in SCC-9 and SCC-15 cells (Fig. 6H). Accordingly, OSC reduced the expression of pro-angiogenic proteins, including HO-1, HIF-1α, and VEGF (Fig. 6I). ZnPP treatment or siHO-1 transfection also markedly decreased the expression of

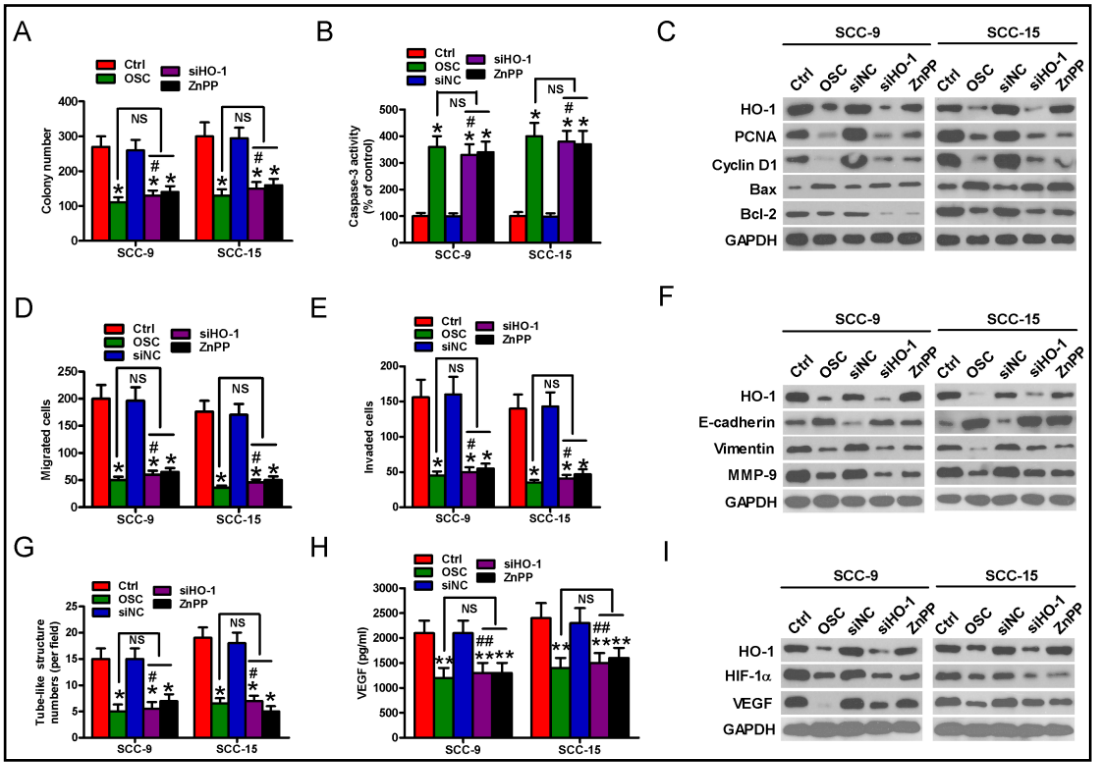

Fig. 6. OSC confers anti-OSCC effects by abolishing HO-1 signaling. (A and B) SCC-9 and SCC-15 cells were treated with vehicle control, OSC (5 μM), siNC, siHO-1, or ZnPP (10 μM) for 24 h. (A) Calculation of colony number. (B) Caspase-3 activity was measured to evaluate cell apoptosis. (C) SCC-9 and SCC-15 cells were treated with vehicle control, OSC (5 μM), or ZnPP (10 μM) for 24 h, or SCC-9 and SCC-15 cells were transfected with siNC or siHO-1 for 48 h. Representative western blotting results of HO-1, PCNA, cyclin D1, Bcl-2, and Bax expression. (D and E) SCC-9 and SCC-15 cells were treated as in (A and B). The numbers of (D) migrated and (E) invaded cells were counted. (F) SCC-9 and SCC-15 cells were treated as in (C). Representative western blotting results of HO-1, E-cadherin, vimentin, and MMP-9 expression. (G) SCC-9 and SCC-15 cells were treated with vehicle control, OSC (5 μM), ZnPP (10 μM), siNC, or siHO-1 for 24 h and the CM was harvested to incubate HUVECs for 36 h. Tube number was determined. (H) SCC-9 and SCC-15 cells were treated as in (A and B). The supernatants were harvested for VEGF measurement by ELISA. (I) SCC-9 and SCC-15 cells were treated as in (C). Western blotting was performed to determine the expression of HO-1, HIF-1α, and VEGF. GAPDH was used as an endogenous control. Data are presented as the mean ± SD of three independent experiments. *P<0.05, **P<0.01 versus Ctrl group, #P<0.05, ##P<0.01 versus siNC group. NS versus OSC group. Ctrl: control; NS: not significant.

HIF-1α and VEGF, consistent with the effects of OSC (Fig. 6I). These results suggest that OSC confers oncostatic effects on OSCC cells by inactivating HO-1 signaling.

OSC hinders tumorigenesis of OSCC in vivo

To investigate whether OSC slows tumorigenesis of OSCC *in vivo*, we established a xenograft mouse model by implanting SCC-9 cells and then intraperitoneally injecting the nude mice with OSC or the vehicle control every 2 days for 3 weeks. As shown in Fig. 7A, OSC treatment markedly inhibited tumor growth compared with the control group. The tumor size of OSC-administered mice was much smaller than in control mice (Fig. 7B). OSC treatment also markedly reduced tumor weight compared with the control group (Fig. 7C). Molecular analyses of the tumor tissues showed that OSC decreased the levels of Nrf2, HO-1, PCNA, cyclin D1, Bcl-2, vimentin, MMP-9, HIF-1α, and VEGF, but increased the expression levels of Bax and E-cadherin, as evidenced by the results of western blotting and IHC assays (Fig. 7D–E). These results demonstrate that OSC inhibits tumorigenesis of OSCC *in vivo*.

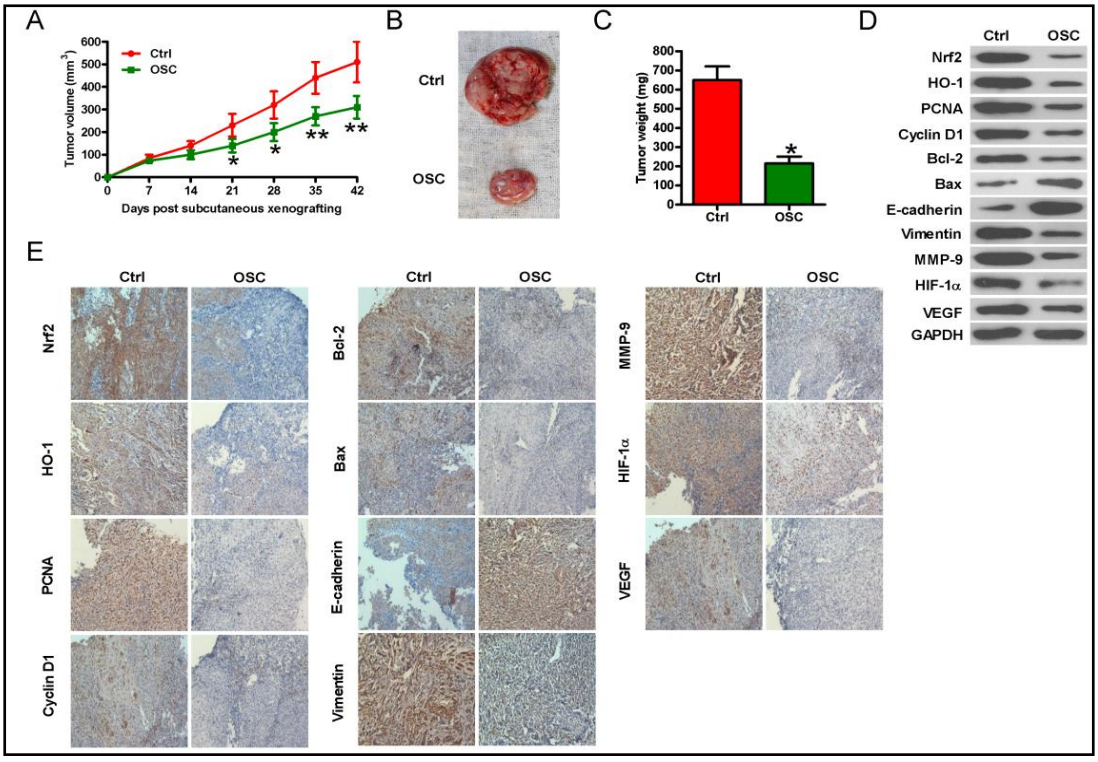

Fig. 7. OSC slowed OSCC tumorigenesis in vivo. Six-week-old BALB/c nude mice were subcutaneously injected with 3 × 10^6 SCC-9 cells. When the tumor size reached approximately 60 mm^3, the mice were administered, by intraperitoneal injection, OSC (80 mg/kg) or the vehicle control every 2 days for 3 weeks. All mice were sacrificed under anesthesia 6 weeks after SCC-9 cell implantation. (A) Tumor volume was monitored once a week for 6 weeks. (B) Images of representative tumors in the two groups. (C) Tumor weight was determined. (D) Western blotting and (E) IHC staining results of Nrf2, HO-1, PCNA, cyclin D1, Bcl-2, Bax, E-cadherin, vimentin, MMP-9, HIF-1α, and VEGF expression. GAPDH was used as an endogenous control. *P<0.05, **P<0.01 versus Ctrl group. Ctrl: control.

Discussion

In this study, we found that OSC slowed tumorigenesis of OSCC *in vitro* and *in vivo*. Key findings were as follows. First, Nrf2 was highly expressed in OSCC tissues and cell lines, and Nrf2 elevation was positively associated with metastases and advanced histological grade and TNM stage, but negatively correlated with differentiation and prognosis of OSCC patients. Second, OSC inhibited activation of the Nrf2/HO-1 signaling pathway in OSCC cells. Third, OSC inhibited proliferation and induced apoptosis of OSCC cells by suppressing HO-1 expression and activation. Fourth, OSC inhibited migration and invasion of OSCC cells by inactivating HO-1 signaling. Fifth, OSC reduced the pro-angiogenic effects of OSCC cells in an HO-1-dependent manner. Finally, OSC reduced tumorigenesis of OSCC *in vivo*. Overall, these results indicate that OSC reduced the proliferation, apoptosis resistance, migration, invasion, and pro-angiogenesis of OSCC cells partly by blocking the Nrf2/HO-1 axis.

As a redox-sensitive transcription factor, Nrf2 controls the expression of various antioxidant and cytoprotective genes and plays a central role in cellular defense [8]. Owing to its cytoprotective functions, Nrf2 has traditionally been considered a tumor suppressor [33, 34]. However, mounting evidence has demonstrated a negative correlation between Nrf2 expression and tumor progression and outcome [16-18, 35]. Nrf2 is highly expressed in gastric cancer [16], non-small-cell lung carcinoma [17], and gallbladder cancer [35],

and upregulation of Nrf2 in these cancer types is closely associated with several clinical characteristics including differentiation, stage, lymph node metastasis, and poor prognosis. Nrf2 expression has been reported to increase in head and neck squamous cell carcinoma [21] and OSCC [22]. The findings in the present study are in accordance with these previous results; the high expression of Nrf2 in OSCC was positively associated with advanced histological grade, TNM stage, and lymph node and distant metastases, and was inversely associated with differentiation and prognosis of OSCC patients.

HO-1, one of the most important effectors of Nrf2, plays crucial roles in the malignant transformation of cancer cells [15, 36]. Aberrant elevations of HO-1 and Nrf2 have been found in many different types of human malignancies, suggesting their oncogenic roles. For instance, a positive correlation was found between the levels of Nrf2 and HO-1 in various cancers [35, 36]. Upregulation of HO-1 increased the aggressiveness of cancer cells, leading to a worse clinical outcome [37]. Indeed, high expression of HO-1 was correlated with advanced stages and poor prognosis of several types of cancers [38-40]. Moreover, HO-1 was highly expressed in OSCC tissues and was associated with lymph node metastasis [41]. Thus, targeting Nrf2/HO-1 axis may be a promising strategy in the treatment of OSCC. In our study, the levels of Nrf2 and HO-1 were much higher in OSCC cells than in hNOKs, and OSC treatment significantly decreased Nrf2 and HO-1 expression in a dose-dependent manner, indicating that OSC could suppress Nrf2/HO-1 signaling in OSCC cells.

Sustained cell proliferation, uncontrolled cell cycle progression, and escape from apoptosis are the significant hallmarks of human cancers [42]. Emerging evidence has shown that high expression of HO-1 promotes cancer cell proliferation [43-45]. Overexpression of HO-1 increased the viability and proliferation of murine melanoma cells *in vitro* and decreased the survival of tumor-bearing mice [46]. HO-1 depletion reduced cell proliferation and induced mitotic delay at G2/M phase in renal carcinoma cells [43]. Incubating chronic myeloid leukemia [44] and ovarian cancer cells [45] with HO-1 inhibitor ZnPP led to the inhibition of cancer cell viability and proliferation. It has been reported that HO-1 has a role in apoptosis resistance in papillary thyroid carcinoma [47], bladder cancer [48], and hepatoma [49]. Knockdown of HO-1 expression using siRNA technology or inhibition of HO-1 activity by ZnPP enhanced apoptosis of many cancer cell types induced by different chemotherapeutic agents [15]. Typical biomarkers of cell proliferation, such as PCNA and cyclin D1, were shown to be ubiquitously highly expressed in OSCC [50, 51]. The apoptosis-associated molecules Bax, Bcl-2, and caspase-3 have been reported to be altered in OSCC [52]. Zhao et al [45]. demonstrated that HO-1 increased Bcl-2 expression and decreased Bax expression, which could be reversed by the inhibition of HO-1 expression in ovarian cancer cells. In the present study, we found that OSC abolished the viability, proliferation, and apoptosis resistance of OSCC cells *in vitro* and slowed tumor growth of OSCC *in vivo*. OSC decreased the expressions of HO-1 PCNA, cyclin D1, and Bcl-2 and increased the levels of Bax in OSCC cells, paralleling the effects of siHO-1 or ZnPP, suggesting that OSC reduced proliferation and induced apoptosis in OSCC cells by suppressing HO-1 signaling.

Local spreading and distant metastasis are the main causes of poor outcome of patients with OSCC [53]. Increased levels of HO-1 in patients with ovarian cancer [45] and non-small-cell lung carcinoma [40] were positively associated with a high metastatic state and poor prognosis. High expression of HO-1 in OSCC specimens was also associated with lymph node metastasis [41]. HO-1 inducer led to enhanced migratory and invasive abilities of ovarian cancer cells, whereas ZnPP incubation significantly inhibited the migration and invasion of ovarian cancer cells [45]. The migratory and invasive abilities of non-small-cell lung carcinoma cells decreased after siHO-1 transfection, but increase after HO-1 overexpression [40]. *In vivo* studies demonstrated that ectopic expression of HO-1 in melanoma cells potentiated cancer aggressiveness and increased lung colonization [46]. Similarly, HO-1-overexpressed pancreatic cancer cells formed more nodules in the lungs after intravenous injection than their wild-type counterparts, whereas reduction of HO-1 activity completely abolished metastasis [54]. Epithelial–mesenchymal transition, loss of epithelial markers such as E-cadherin, and gain of mesenchymal markers such as vimentin

are essential for tumor spreading and dissemination [55]. In ovarian cancer cells, ZnPP treatment caused obvious downregulation of vimentin [45]. It has been reported that HO-1 increased the expression of metastasis-associated protein MMP-9 in non-small-cell lung carcinoma cells [40]. Here, we demonstrated that OSC treatment markedly reduced OSCC cell migration and invasion *in vitro*. OSC downregulated the levels of HO-1, vimentin, and MMP-9 and upregulated E-cadherin expression in OSCC cells, which was consistent with the results of siHO-1 or ZnPP treatment. These data indicated that OSC targets HO-1 signaling to hinder the migration and invasion of OSCC cells.

Angiogenesis is essential not only for tumor growth but also for metastasis [42]. The pro-angiogenic roles of HO-1 are directly evidenced in human pancreatic cancer [54], murine melanoma [46], and murine lung cancer [56]. HO-1 stimulated angiogenesis to accelerate pancreatic carcinoma growth in a mouse model [54]. Tumors derived from mice injected with HO-1-overexpressed melanoma cells displayed excessive vascularization and increased VEGF production [46]. Moreover, ZnPP administration decreased microvessel density and VEGF generation in LL/2 lung cancer in mice [56]. It has been reported that increased HO-1 is positively correlated with elevated expression of HIF-1α and high microvessel density in clinical specimens of bladder cancer [57]. Inhibition of HO-1 by ZnPP decreased the growth and microvessel density of T24 tumors, which may be partly attributed to the suppression of pro-angiogenic factors, particularly VEGF and HIF-1α [57]. In the present study, OSC treatment clearly inhibited the pro-angiogenic effects of OSCC cells and the release of VEGF from OSCC cells *in vitro*. OSC reduced the levels of HO-1, VEGF, and HIF-1α in OSCC cells, similar to the effects of siHO-1 or ZnPP. These results suggest that OSC suppressed HO-1-mediated pro-angiogenesis of OSCC cells.

Several limitations of this study should be considered. First, we demonstrated that OSC reduced Nrf2/HO-1-dependent proliferation, mobility, and pro-angiogenesis of OSCC cells *in vitro* only by conducting inhibitory experiments using siRNA or ZnPP treatment. It would be interesting to further explore the rescue effects of HO-1 overexpression on OSC-treated OSCC cells. Second, we found that OSC hindered the proliferation, migration, invasion, and pro-angiogenesis of OSCC cells *in vitro* by inactivating HO-1 signaling; however, we only probed that OSC retards tumorigenesis of OSCC *in vivo*, involving the expression changes of HO-1 and its downstream molecules. Thus, further investigation is required to elucidate whether OSC suppression of OSCC carcinogenesis is directly dependent on HO-1 signaling. In future studies, we aim to construct an OSCC cell line with stable HO-1 depletion to establish a xenograft mouse model. Then, we will explore whether the inhibitory effects of OSC on OSCC directly rely on HO-1 signaling, similar to the *in vitro* findings.

Conclusion

In summary, our study provides evidence that OSC represses Nrf2/HO-1- dependent growth, metastasis, and pro-angiogenesis of OSCC. We found that Nrf2 was highly expressed in OSCC tissues and cell lines. Nrf2 elevation was positively correlated with growth, metastasis, and poor outcome of OSCC. Functional experiments revealed that OSC decreased proliferation, migration, invasion, and pro-angiogenesis, and increased the apoptosis of OSCC cells, in part by targeting the Nrf2/HO-1 axis. Therefore, OSC may be a potential therapeutic agent for OSCC.

Acknowledgements

This study was supported by grants from the Open Project for State Key Laboratory of Military Stomatology (No. 2016KA03), the Open Project of the State Key Laboratory of Trauma, Burn and Combined Injury, Third Military Medical University (No. SKLKF201708), the Science and Technology Foundation of Chongqing, China (No. cstc2014jcyjA10092), and

the Postdoctoral Science Foundation of Chongqing (No. Xm2015099). The funding sources played no role in the study design, collection, analysis, or interpretation of data, writing of the report, or decision to publish.

Disclosure Statement

The authors have no conflicts of interest to declare.

References

1 Ferlay J, Soerjomataram I, Dikshit R, Eser S, Mathers C, Rebelo M, Parkin DM, Forman D, Bray F. Cancer incidence and mortality worldwide: Sources, methods and major patterns in globocan 2012. Int J Cancer 2015;136:E359–386.
2 Scully C, Bagan J. Oral squamous cell carcinoma overview. Oral Oncol 2009;45:301–3088.
3 Leemans CR, Braakhuis BJ, Brakenhoff RH. The molecular biology of head and neck cancer. Nat Rev Cancer 2011;11:9–22.
4 Johnson N. Tobacco use and oral cancer: A global perspective. J Dent Educ 2001;65:328–339.
5 Wang B, Zhang S, Yue K, Wang XD. The recurrence and survival of oral squamous cell carcinoma: A report of 275 cases. Chin J Cancer 2013;32:614–618.
6 Leemans CR, Tiwari R, Nauta JJ, van der Waal I, Snow GB. Recurrence at the primary site in head and neck cancer and the significance of neck lymph node metastases as a prognostic factor. Cancer 1994;73:187–190.
7 Noguti J, De Moura CF, De Jesus GP, Da Silva VH, Hossaka TA, Oshima CT, Ribeiro DA. Metastasis from oral cancer: An overview. Cancer Genomics Proteomics 2012;9:329–335.
8 Li W, Kong AN. Molecular mechanisms of Nrf2-mediated antioxidant response. Mol Carcinog 2009;48:91–104.
9 Cullinan SB, Gordan JD, Jin J, Harper JW, Diehl JA. The Keap1-BTB protein is an adaptor that bridges Nrf2 to a Cul3-based E3 ligase: oxidative stress sensing by a Cul3-Keap1 ligase. Mol Cell Biol 2004;24:8477–8486.
10 Malhotra D, Portales-Casamar E, Singh A, Srivastava S, Arenillas D, Happel C, Shyr C, Wakabayashi N, Kensler TW, Wasserman WW, Biswal S. Global mapping of binding sites for Nrf2 identifies novel targets in cell survival response through CHIP-Seq profiling and network analysis. Nucleic Acids Res 2010;38:5718–5734.
11 Chorley BN, Campbell MR, Wang X, Karaca M, Sambandan D, Bangura F, Xue P, Pi J, Kleeberger SR, Bell DA. Identification of novel NRF2-regulated genes by CHIP-Seq: influence on retinoid X receptor alpha. Nucleic Acids Res 2012;40:7416–7429.
12 Hayes JD, Dinkova-Kostova AT. The Nrf2 regulatory network provides an interface between redox and intermediary metabolism. Trends Biochem Sci 2014;39:199–218.
13 Ohkoshi A, Suzuki T, Ono M, Kobayashi T, Yamamoto M. Roles of Keap1-Nrf2 system in upper aerodigestive tract carcinogenesis. Cancer Prev Res (Phila) 2013;6:149–159.
14 Gañán-Gómez I, Wei Y, Yang H, Boyano-Adánez MC, García-Manero G. Oncogenic functions of the transcription factor Nrf2. Free Radic Biol Med 2013;65:750–764.
15 Na HK, Surh YJ. Oncogenic potential of Nrf2 and its principal target protein heme oxygenase-1. Free Radic Biol Med 2014;67:353–365.
16 Kawasaki Y, Ishigami S, Arigami T, Uenosono Y, Yanagita S, Uchikado Y, Kita Y, Nishizono Y, Okumura H, Nakajo A, Kijima Y, Maemura K, Natsugoe S. Clinicopathological significance of nuclear factor (erythroid-2)-related factor 2 (Nrf2) expression in gastric cancer. BMC Cancer 2015;15:5.
17 Solis LM, Behrens C, Dong W, Suraokar M, Ozburn NC, Moran CA, Corvalan AH, Biswal S, Swisher SG, Bekele BN, Minna JD, Stewart DJ, Wistuba II. Nrf2 and Keap1 abnormalities in non-small cell lung carcinoma and association with clinicopathologic features. Clin Cancer Res 2010;16:3743–3753.

18 Chien MH, Lee WJ, Hsieh FK, Li CF, Cheng TY, Wang MY, Chen JS, Chow JM, Jan YH, Hsiao M, Hua KT, Kuo ML. Keap1-Nrf2 interaction suppresses cell motility in lung adenocarcinomas by targeting the S100P protein. Clin Cancer Res 2015;21:4719–4732.
19 Zhang C, Wang HJ, Bao QC, Wang L, Guo TK, Chen WL, Xu LL, Zhou HS, Bian JL, Yang YR, Sun HP, Xu XL, You QD. Nrf2 promotes breast cancer cell proliferation and metastasis by increasing RhoA/ROCK pathway signal transduction. Oncotarget 2016;7:73593–73606.
20 Fan Z, Wirth AK, Chen D, Wruck CJ, Rauh M, Buchfelder M, Savaskan N. Nrf2-Keap1 pathway promotes cell proliferation and diminishes ferroptosis. Oncogenesis 2017;6:e371.
21 Stacy DR, Ely K, Massion PP, Yarbrough WG, Hallahan DE, Sekhar KR, Freeman ML. Increased expression of nuclear factor E2 p45-related factor 2 (NRF2) in head and neck squamous cell carcinomas. Head Neck 2006;28:813–818.
22 Huang CF, Zhang L, Ma SR, Zhao ZL, Wang WM, He KF, Zhao YF, Zhang WF, Liu B, Sun ZJ. Clinical significance of Keap1 and Nrf2 in oral squamous cell carcinoma. PloS One 2013;8:e83479.
23 Fan H, Paiboonrungruan C, Zhang X, Prigge JR, Schmidt EE, Sun Z, Chen X. Nrf2 regulates cellular behaviors and notch signaling in oral squamous cell carcinoma cells. Biochem Biophys Res Commun 2017;493:833–839.
24 Song JZ, Xu HX, Tian SJ, But PP. Determination of quinolizidine alkaloids in traditional chinese herbal drugs by nonaqueous capillary electrophoresis. J Chromatogr A 1999;857:303–311.
25 Xu T, Li Y, Wang H, Xu Y, Ma L, Sun T, Ma H, Yu J. Oxysophocarpine induces anti-nociception and increases the expression of gabaaalpha1 receptors in mice. Mol Med Rep 2013;7:1819–1825.
26 Zhu QL, Li YX, Zhou R, Ma NT, Chang RY, Wang TF, Zhang Y, Chen XP, Hao YJ, Jin SJ, Ma L, Du J, Sun T, Yu JQ. Neuroprotective effects of oxysophocarpine on neonatal rat primary cultured hippocampal neurons injured by oxygen-glucose deprivation and reperfusion. Pharm Biol 2014;52:1052–1059.
27 Zhao P, Chang RY, Liu N, Wang J, Zhou R, Qi X, Liu Y, Ma L, Niu Y, Sun T, Li YX, He YP, Yu JQ. Neuroprotective effect of oxysophocarpine by modulation of mapk pathway in rat hippocampal neurons subject to oxygen-glucose deprivation and reperfusion. Cell Mol Neurobiol 2018;38:529–540.
28 Yang Y, Li YX, Wang HL, Jin SJ, Zhou R, Qiao HQ, Du J, Wu J, Zhao CJ, Niu Y, Sun T, Yu JQ. Oxysophocarpine ameliorates carrageenan-induced inflammatory pain via inhibiting expressions of prostaglandin E2 and cytokines in mice. Planta Med 2015;81:791–797.
29 Pan QM, Li YH, Hua J, Huang FP, Wang HS, Liang D. Antiviral matrine-type alkaloids from the Rhizomes of Sophora tonkinensis. J Nat Prod 2015;78:1683–1688.
30 Gao J, Li Y, Wang Q, Ma X, Zhang Y. Oxysophocarpine inhibits lung injury induced by respiratory syncytial virus. Am J Transl Res 2017;9:4083–4093.
31 Zhang L, Li G, Houghton PJ, Jackson S, Twentyman PR. Alkaloids in Sophora alopecuroides seed and relevant tests for activity. Zhongguo Zhong Yao Za Zhi 1997;22:740–764.
32 Wang Q, Xu J, Li X, Zhang D, Han Y, Zhang X. Comprehensive two-dimensional PC-3 prostate cancer cell membrane chromatography for screening anti-tumor components from Radix Sophorae flavescentis. J Sep Sci 2017;40:2688–2693.
33 Ramos-Gomez M, Kwak MK, Dolan PM, Itoh K, Yamamoto M, Talalay P, Kensler TW. Sensitivity to carcinogenesis is increased and chemoprotective efficacy of enzyme inducers is lost in nrf2 transcription factor-deficient mice. Proc Natl Acad Sci U S A 2001;98:3410–3415.
34 Rachakonda G, Sekhar KR, Jowhar D, Samson PC, Wikswo JP, Beauchamp RD, Datta PK, Freeman ML. Increased cell migration and plasticity in Nrf2-deficient cancer cell lines. Oncogene 2010;29:3703–3714.
35 Wang J, Zhang M, Zhang L, Cai H, Zhou S, Zhang J, Wang Y. Correlation of Nrf2, HO-1, and MRP3 in gallbladder cancer and their relationships to clinicopathologic features and survival. J Surg Res 2010;164:e99–105.
36 Furfaro AL, Traverso N, Domenicotti C, Piras S, Moretta L, Marinari UM, Pronzato MA, Nitti M. The Nrf2/HO-1 axis in cancer cell growth and chemoresistance. Oxid Med Cell Longev 2016;2016:1958174.
37 Jozkowicz A, Was H, Dulak J. Heme oxygenase-1 in tumors: Is it a false friend? Antioxid Redox Signal 2007;9:2099–2117.
38 Miyake M, Fujimoto K, Anai S, Ohnishi S, Nakai Y, Inoue T, Matsumura Y, Tomioka A, Ikeda T, Tanaka N, Hirao Y. Clinical significance of heme oxygenase-1 expression in non-muscle-invasive bladder cancer. Urol Int 2010;85:355–363.

39 Degese MS, Mendizabal JE, Gandini NA, Gutkind JS, Molinolo A, Hewitt SM, Curino AC, Coso OA, Facchinetti MM. Expression of heme oxygenase-1 in non-small cell lung cancer (NSCLC) and its correlation with clinical data. Lung Cancer 2012;77:168–175.
40 Tsai JR, Wang HM, Liu PL, Chen YH, Yang MC, Chou SH, Cheng YJ, Yin WH, Hwang JJ, Chong IW. High expression of heme oxygenase-1 is associated with tumor invasiveness and poor clinical outcome in non-small cell lung cancer patients. Cell Oncol (Dordr) 2012;35:461–471.
41 Lee SS, Yang SF, Tsai CH, Chou MC, Chou MY, Chang YC. Upregulation of heme oxygenase-1 expression in areca-quid-chewing-associated oral squamous cell carcinoma. J Formos Med Assoc 2008;107:355–363.
42 Hanahan D, Weinberg RA. Hallmarks of cancer: The next generation. Cell 2011;144:646–674.
43 Lin PH, Lan WM, Chau LY. TRC8 suppresses tumorigenesis through targeting heme oxygenase-1 for ubiquitination and degradation. Oncogene 2013;32:2325–2334.
44 Mayerhofer M, Florian S, Krauth MT, Aichberger KJ, Bilban M, Marculescu R, Printz D, Fritsch G, Wagner O, Selzer E, Sperr WR, Valent P, Sillaber C. Identification of heme oxygenase-1 as a novel BCR/ABL-dependent survival factor in chronic myeloid leukemia. Cancer Res 2004;64:3148–3154.
45 Zhao Z, Xu Y, Lu J, Xue J, Liu P. High expression of HO-1 predicts poor prognosis of ovarian cancer patients and promotes proliferation and aggressiveness of ovarian cancer cells. Clin Transl Oncol 2018;20:491–499.
46 Was H, Cichon T, Smolarczyk R, Rudnicka D, Stopa M, Chevalier C, Leger JJ, Lackowska B, Grochot A, Bojkowska K, Ratajska A, Kieda C, Szala S, Dulak J, Jozkowicz A. Overexpression of heme oxygenase-1 in murine melanoma: Increased proliferation and viability of tumor cells, decreased survival of mice. Am J Pathol 2006;169:2181–2198.
47 Chen GG, Liu ZM, Vlantis AC, Tse GM, Leung BC, van Hasselt CA. Heme oxygenase-1 protects against apoptosis induced by tumor necrosis factor-alpha and cycloheximide in papillary thyroid carcinoma cells. J Cell Biochem 2004;92:1246–1256.
48 Kocanova S, Buytaert E, Matroule JY, Piette J, Golab J, de Witte P, Agostinis P. Induction of heme-oxygenase 1 requires the p38MAPK and PI3K pathways and suppresses apoptotic cell death following hypericin-mediated photodynamic therapy. Apoptosis 2007;12:731–741.
49 Liu YS, Li HS, Qi DF, Zhang J, Jiang XC, Shi K, Zhang XJ, Zhang XH. Zinc protoporphyrin IX enhances chemotherapeutic response of hepatoma cells to cisplatin. World J Gastroenterol 2014;20:8572–8582.
50 Poosarla C, Ramesh M, Ramesh K, Gudiseva S, Bala S, Sundar M. Proliferating cell nuclear antigen in premalignancy and oral squamous cell carcinoma. J Clin Diagn Res 2015;9:Zc39–41.
51 Das SN, Khare P, Singh MK, Sharma SC. Correlation of cyclin D1 expression with aggressive DNA pattern in patients with tobacco-related intraoral squamous cell carcinoma. Indian J Med Res 2011;133:381–386.
52 Uchida M, Iwase M, Takaoka S, Yoshiba S, Kondo G, Watanabe H, Ohashi M, Nagumo M, Shintani S. Enhanced susceptibility to tumor necrosis factor-related apoptosis-inducing ligand-mediated apoptosis in oral squamous cell carcinoma cells treated with phosphatidylinositol 3-kinase inhibitors. Int J Oncol 2007;30:1163–1171.
53 Kowalski LP, Bagietto R, Lara JR, Santos RL, Silva JF Jr., Magrin J. Prognostic significance of the distribution of neck node metastasis from oral carcinoma. Head Neck 2000;22:207–214.
54 Sunamura M, Duda DG, Ghattas MH, Lozonschi L, Motoi F, Yamauchi J, Matsuno S, Shibahara S, Abraham NG. Heme oxygenase-1 accelerates tumor angiogenesis of human pancreatic cancer. Angiogenesis 2003;6:15–24.
55 Cannito S, Novo E, di Bonzo LV, Busletta C, Colombatto S, Parola M. Epithelial-mesenchymal transition: From molecular mechanisms, redox regulation to implications in human health and disease. Antioxid Redox Signal 2010;12:1383–1430.
56 Hirai K, Sasahira T, Ohmori H, Fujii K, Kuniyasu H. Inhibition of heme oxygenase-1 by zinc protoporphyrin IX reduces tumor growth of LL/2 lung cancer in C57BL mice. Int J Cancer 2007;120:500–505.
57 Miyake M, Fujimoto K, Anai S, Ohnishi S, Kuwada M, Nakai Y, Inoue T, Matsumura Y, Tomioka A, Ikeda T, Tanaka N, Hirao Y. Heme oxygenase-1 promotes angiogenesis in urothelial carcinoma of the urinary bladder. Oncol Rep 2011;25:653–660.